Variability of the South Pacific western Subtropical Mode Water and its relationship with ENSO during the Argo period

Jifeng Qi[1,2,3], Tangdong Qu[2*], Baoshu Yin[1,3,4*], Jianwei Chi[5]

[1]CAS Key Laboratory of Ocean Circulation and Waves, Institute of Oceanology, Chinese Academy of Sciences, and Pilot National Laboratory for Marine Science and Technology (Qingdao), Qingdao, China

[2]Joint Institute for Regional Earth System Science and Engineering, University of California, Los Angeles, Los Angeles, California

[3]Center for Ocean Mega-Science, Chinese Academy of Sciences, Qingdao, China

[4]University of Chinese Academy of Sciences, Beijing, China

[5]State Key Laboratory of Tropical Oceanography, South China Sea Institute of Oceanology, Chinese Academy of Sciences, Guangzhou, China.

Corresponding author: T. Qu (tangdong@ucla.edu); B. Yin (bsyin@qdio.ac.cn)

Key Points:

- A gridded Argo dataset is used to study variability of the South Pacific western subtropical mode water (SPWSTMW) over 2004-2019.
- The SPWSTMW volume varies on various timescales, and this variability is mainly caused by change in winter mixed layer depth.
- Anomalous winds associated with ENSO are largely responsible for the interannual variability of the SPWSTMW volume.

Abstract

This study investigates variability of the South Pacific western Subtropical Mode Water (SPWSTMW), its physical processes and relationship with ENSO, using a gridded Argo data product from January 2004 to September 2019. On seasonal timescale, the SPWSTMW volume shows a significant variability, which involves three periods: the formation period (June-October), the isolation period (November-February), and the dissipation period (March-May). This seasonal variability is related to seasonal fluctuation of the mixed layer depth. During the Argo period from 2004 to 2019, interannual variability of the SPWSTMW volume is tightly linked to the El Niño-Southern Oscillation (ENSO), increasing during El Niño periods and decreasing during La Niña periods. Further analyses indicate that ENSO-related anomalous winds are primarily responsible for interannual variability of the SPWSTMW volume. The anomalous winds first influence the surface heat flux through evaporation and then the mixed layer depth through convection, leaving an imprint of ENSO on the SPWSTMW. This study also shows that the SPWSTMW responds differently to the central Pacific (CP) El Niño and eastern Pacific (EP) El Niño.

Keywords: Subtropical mode water; Southwest Pacific Ocean; ENSO; Mixed layer depth

Plain Language Summary

Using recently available Argo dataset and atmospheric reanalysis products, this study investigates the impact of ENSO on the volume of the South Pacific western subtropical mode water (SPWSTMW) and its underlying mechanisms. The results show that interannual variability of the SPWSTMW volume has a strong ENSO signal during the Argo period from 2004 to 2019, which is mainly forced by ENSO-induced wind anomalies. During El Niño years, surface winds in the SPWSTMW formation region are stronger than during normal years, resulting in a decrease in sea surface temperature (SST) through the wind-evaporation-SST (WES) feedback. The reduced SST can decrease the stratification and deepens the MLD, which enhances the horizontal MLD gradients and consequently the lateral induction and subduction of the SPWSTMW, directly contributing to the increase of the SPWSTMW volume. This study provides new insights into our understanding of regional oceanography and climate change in the South Pacific.

1 Introduction

Subtropical Mode Water (STMW), characterized by low potential vorticity (i.e., a thermostad or pycnostad) occurring between the seasonal and permanent pycnocline, is present in all subtropical gyres of the global ocean (Hanawa & Talley, 2001). It is formed by surface cooling and convective mixing during cool seasons. After its formation, the STMW spreads in a wide region of the subtropical gyre as a result of advection and eddy activity. Since the STMW retains the memory of atmospheric conditions and conveys the surface signals into the subsurface ocean, its variability has been shown to have notable impacts on climate variability and upper-ocean dynamics on multiple time scales, providing a direct link between the atmosphere and the ocean (Huang & Qiu, 1998; Ladd & Thompson, 2000; Xie et al., 2011; Oka et al., 2015; Yu et al., 2015).

The STMW has been extensively studied throughout the global ocean over the past few decades (Roemmich & Cornuelle, 1992; Hanawa & Talley, 2001; Holbrook & Maharaj, 2008; Oka & Qiu, 2012; Speer & Forget, 2013; Fernandez et al., 2017). However, compared with its northern hemisphere counterpart, fewer studies have focused on the STMW in the southern hemisphere oceans. The main reason is that southern subtropical gyres are less sampled than the northern ones, and thus STMW has been, so far, detected in small amount. Recently, as more observational data products, such as the Digital Atlas of Southwest Pacific upper Ocean Temperatures (DASPOT) (Holbrook & Bindoff, 2000 a, b) and the Argo gridded dataset (Roemmich & Gilson, 2009), became available, the STMW in the south Pacific Ocean has received increasing attention (Holbrook & Maharaj, 2008; Sato & Suga, 2009; Fernandez et al., 2017). A good example of this is the STMW in the southwestern Pacific (SPWSTMW) lying to the north of the Tasman Front. Zonally, the SPWSTMW extends from the east coast of Australia to about 170°W, with a temperature range of 14-20 °C and a density range of 25.25-26.5 kg/m^3 (Roemmich & Cornuelle, 1992; Holbrook & Maharaj, 2008). Studies of the SPWSTMW have recently focused on its role as a heat reservoir in memorizing the wintertime atmospheric conditions in its formation region (Holbrook & Maharaj, 2008; Wang et al., 2015; Fernandez et al., 2017).

The SPWSTMW was first identified by Roemmich and Cornuelle (1992) on the basis of hydrographic data collected between New Zealand and Fiji. They revealed that the SPWSTMW is formed by convective mixing during the austral winter in the eastward-flowing waters of the East Australia Current (EAC) with a potential temperature range of 15-19 ℃ and vertical temperature gradient no more than 2 ℃/100m. Roemmich and Cornuelle (1992) attributed the SPWSTMW variability to two probable factors: 1) anomalous sea surface heat fluxes; and 2) anomalous heat transport by ocean currents. A similar conclusion was reached by Roemmich et al. (2005). However, Sprintall et al. (1995) pointed out that the SPWSTMW variability is mainly due to anomalous oceanic heat transport, not due to anomalous surface heat flux. Based on World Ocean Atlas (WOA) 2001 climatology and high-resolution expendable bathythermograph (HRX) line data, Tsubouchi et al. (2007) divided the SPWSTMW into three types: the West type, located in the EAC recirculation region, the North type, located to the north of the Tasman Front extension, and the South type, located to the south of the Tasman Front extension. By using the DASPOT dataset for the period 1973-1988, a systematic study on the SPWSTMW has been conducted by Holbrook and Maharaj (2008). They found that the SPWSTMW extends across the entire width of the southwestern Pacific, with a remarkable seasonal and interannual variability. They demonstrated that El Niño-Southern Oscillation (ENSO) plays an important role in the interannual variability of the SPWSTMW. Their results also suggested that the STMW in the western South Pacific exhibits different behaviors over different parts of the region. Most recently, Fernandez et al. (2017) found that larger volume of the SPWSTMW is associated with cooler conditions in the formation region. In most cases, the SPWSTMW inventory tends to increase (decrease) with strengthening (weakening) western boundary current north of New Zealand.

Using the Bluelink ReANalysis 2.1 dataset, Wang et al. (2015) claimed that, on seasonal timescale, surface heat flux is dominant in governing the SPWSTMW variability. But, on interannual timescales, surface heat flux and ocean dynamics are of equal importance. According to Wang et al. (2015), the total SPWSTMW volume west of 180° varies seasonally between a maximum of 7.8 (±0.5) $\times 10^{14}$ m^3 in September and a minimum of 1.6 (±0.4) $\times 10^{14}$ m^3 in March. This amplitude of seasonal variability is slightly larger than that between 6.6 (±0.5) $\times 10^{14}$ m^3 in October and 1.9 (±0.4) $\times 10^{14}$ m^3 in May reported by Holbrook and Maharaj (2008) based on the DASPOT dataset.

The El Niño-Southern Oscillation (ENSO) is one of the most prominent modes of large-scale variability in the global ocean (Alexander et al., 2002; McPhaden et al., 2006; Taschetto & England, 2009; Taschetto et al., 2014; Yu et al., 2017; Freund et al., 2019). The ENSO-induced changes in ocean circulation and air-sea fluxes over the South Pacific are believed to directly contribute to the SPWSTMW variability (Roemmich & Cornuelle, 1992; Holbrook & Maharaj, 2008; Wang et al., 2015; Fernandez et al., 2017). For example, Holbrook and Maharaj (2008) claimed that the anomalous cooling of the Southwest Pacific Ocean during El Niño periods can enhance winter time convection, which leads to more SPWSTMW formed in the region. A similar conclusion was reached by Fernandez et al. (2017). However, Wang et al. (2015) claimed that the SPWSTMW formation can be further enhanced by La Niña, which drives positive anomalies in sea surface salinity in the southwest Pacific Ocean and creates a favorable preconditioning for surface cooling in the austral winter.

Despite the fact that much effort has been made in investigating variability of the SPWSTMW, some processes governing evolution of the SPWSTMW are still debated and need to be investigated further. For example, previous studies suggested that the anomalous cooling in the Southwest Pacific associated with ENSO can lead to more SPWSTMW formed (Holbrook & Maharaj, 2008; Fernandez et al., 2017). However, the exact mechanisms responsible for this ENSO-SPWSTMW teleconnection have not been fully studied. Recently, a new type of El Niño, referred to as El Niño-Modoki (Ashok et al., 2007; Freund et al. 2019), or central Pacific (CP) El Niño (Yu & Kim, 2010) has been identified, in which maximum sea surface temperature (SST) anomalies are confined mostly in the central Pacific, different from the conventional Eastern Pacific (EP) El Niño with maximum SST anomalies occurred in the east Pacific. Whether the SPWSTMW responds differently to the CP El Niño and EP El Niño is also an interesting question worthy of further study.

The present study uses a recently available Argo dataset and reanalysis datasets to examine the variability of the SPWSTMW. An important contribution of this paper is to demonstrate the dominant role of the ENSO-induced wind anomalies in

SPWSTMW variability on interannual timescales. The rest of this paper is organized as follows. The data and methods of analysis are presented in Section 2. Basic characteristics of the SPWSTMW and its seasonal variability are discussed in Section 3. Interannual variability of the SPWSTMW volume and its relationship to ENSO are discussed in Section 4. Finally, a discussion of the finding is presented in Section 5.

2 Data and Methods

2.1 Data

The gridded Argo data product from January 2004 to September 2019 created by Roemmich and Gilson (2009) (hereinafter referred to as RG09) is used to investigate the SPWSTMW variability, especially with regard to its relationship with ENSO. The RG09 data product provides 1-degree gridded monthly temperature and salinity fields with 58 vertical levels from the sea surface to 2000 dbar. This dataset has been used by many previous studies (e.g., Drushka et al., 2014; Fernandez et al., 2017). For more details, the reader is referred to Roemmich and Gilson (2009) and the link provided in the Acknowledgements.

Monthly surface heat flux product with a horizontal resolution of 2.5°×2.5° was obtained from the National Centers for Environmental Prediction (NCEP) re-analyses (Kalnay et al., 1996). This reanalysis product was interpolated into a 1°×1° grid, with the same horizontal grid as the Argo data product. Positive values of surface heat flux indicate the ocean gaining heat from atmosphere, while negative values represent the opposite. Also used for the present study is a monthly surface wind product on a 1°×1° grid from ERA-Interim produced by the European Centre for Medium-Range Weather

Forecasts (ECMWF) (Dee et al., 2011). The monthly Southern Oscillation Index (SOI) was obtained from the Australian Government Bureau of Meteorology and is used to characterize the ENSO signal.

2.2 Definition of the SPWSTMW

As a key factor influencing the SPWSTMW, we first define the mixed layer depth (MLD) as the depth where water is denser than the surface water by 0.125 kg/m^3, which has been used in previous studies (e.g., Huang & Qiu, 1998). The all-time (2004-2019) mean MLD in the subtropical South Pacific derived from the RG09 data product is shown in Figure 1a. Its spatial pattern is dominated by a significant MLD front (indicated by the 80 m contour) in the western South Pacific, and a local MLD maximum (> 80 m) in the eastern South Pacific, corresponding to the formation region of the western and eastern STMW, respectively (Wong & Johnson, 2003; Li, 2012; Fernandez et al., 2017). Averaged over the region (0°-50°S, 145°E-70°W), the MLD reaches its seasonal maximum (130 m) in August and minimum (33 m) in January (Figure 1b).

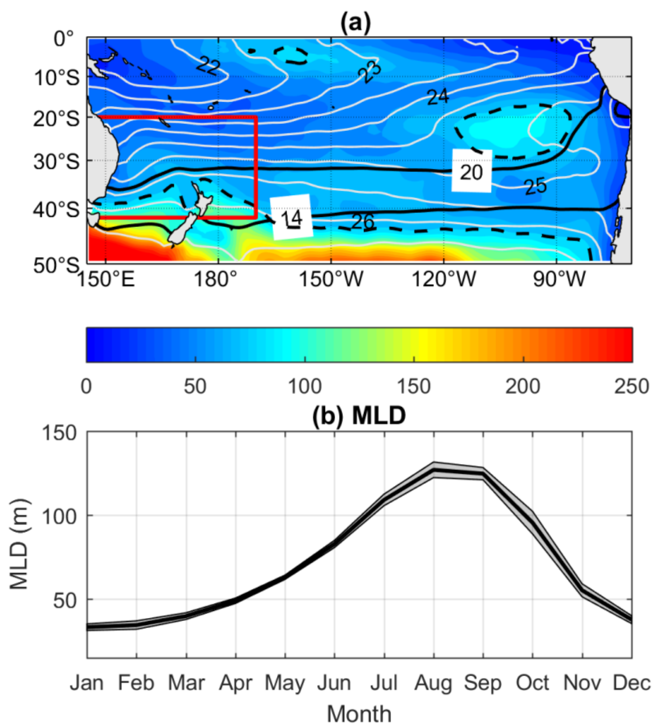

Figure 1. (a) All-time mean depth (color in m) and potential density (contour in kg/m^3) of mixed layer from RG09 data product. The black dashed line (80 m contour) represents the location of the MLD front, the black solid lines show the 14 ℃ and 20 ℃ isotherms, and the red thick box indicates the study region. (b) Seasonal variation of the MLD averaged over the region (0°-50°S, 145°E-70°W). The gray shading indicates the standard deviation of the MLD.

We then define the SPWSTMW as a minimum of vertical temperature gradient, as has been done by several earlier studies (Roemmich & Cornuelle, 1992; Holbrook & Maharaj, 2008; Wang et al., 2015; Fernandez et al., 2017). To evaluate the minimum of the vertical temperature gradient of the SPWSTMW, we examine all gridded temperature/salinity profiles in the region (20°S-42°S, 150°E-170°W) during September-December from 2004 to 2018. The result shows that the majority of temperature/salinity profiles have a minimum of vertical temperature gradient less than 1.8 ℃/100m (Figure 2a). This threshold of vertical temperature gradient is therefore selected as the criterion to define the SPWSTMW. We also examined the potential temperature, salinity, and potential density of the SPWSTMW in the region studied. In most cases, the SPWSTMW lies between 14°C and 20°C in potential temperature, between 35.3 and 35.7 psu in salinity and between 25.25 and 26.5 kg /m^3 in potential density. These properties of the SPWSTMW are consistent with earlier studies (Roemmich & Cornuelle, 1992; Tsubouchi et al., 2007). Similar to Holbrook and Maharaj (2008), errors of the SPWSTMW shown in the present study are calculated as the upper and lower bounds estimates on the SPWSTMW thickness and total volume.

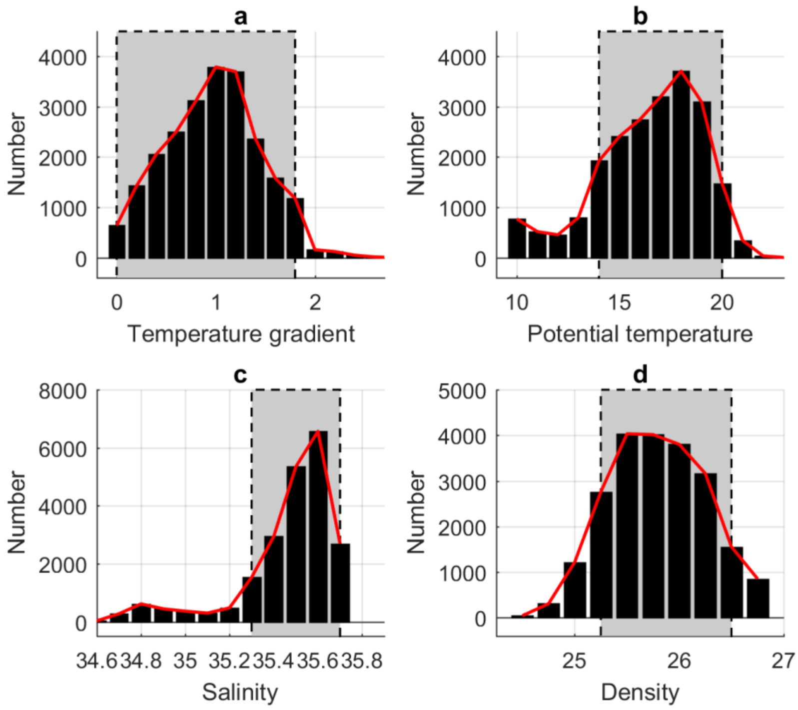

Figure 2. Histogram of number of gridded temperature/salinity profiles with respect to (a) core layer temperature gradient (°C/100m), (b) potential temperature (°C), (c) salinity (psu), and (d) potential density (kg/m^3) of the SPWSTMW in the region (20°S-42°S, 150°E-170°W) during September-December from 2004 to 2018.

3 Results

The climatological temperature and salinity data are used to identify the presence of the SPWSTMW. If identified, depths of the upper and lower limits of the SPWSTMW can be determined. Figure 3 shows the spatial distribution of these depths. In general, depth of the upper limit of the SPWSTMW is shallower in the south (Figure 3a). It gradually increases to the north from about 110 m at 40°S to about 190 m at 20°S. Depth of the lower limit shows two maxima at latitudes between 28°S and 35°S, both exceeding 270 m in magnitude (Figure 3b). The thickness of the SPWSTMW is then obtained as the depth difference between the lower and upper limits, where the SPWSTMW is identified (Figure 3c).

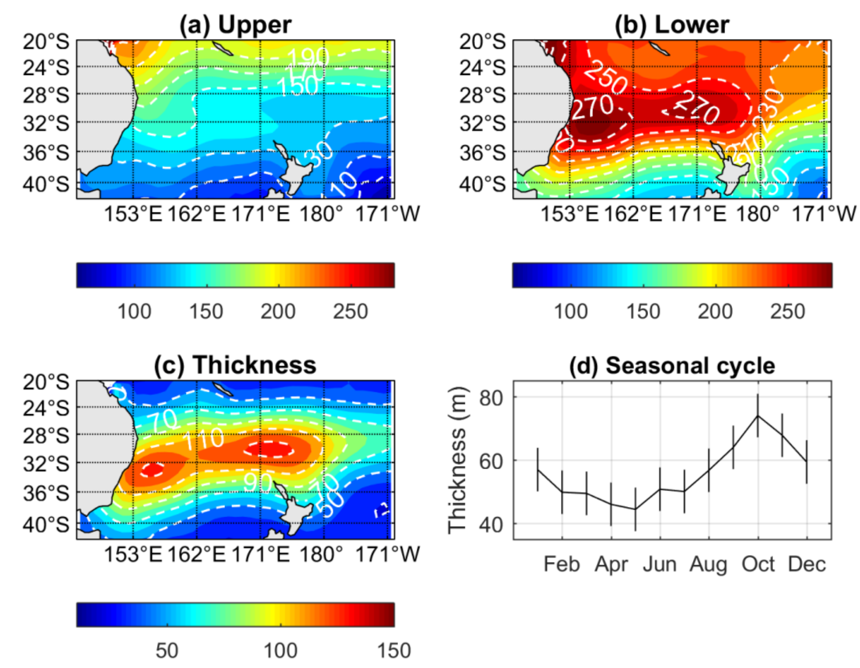

Figure 3. Depth of the (a) upper and (b) lower limits of the SPWSTMW and (c) its layer thickness identified by the RG09 data product. Included in (d) is the mean seasonal cycle of the SPWSTMW thickness, calculated by averaging over all grid points where the SPWSTMW is identified. The vertical bars represent thickness errors (units: m).

In general, the climatological thickness of the SPWSTMW is greater than 50 m (Figure 3c). Averaged over the region studied, it reaches 62±(10) m. A thick layer of the SPWSTMW (exceeding 80 m) is seen extending eastward from the east Australian coast along the southern rim of the subtropical gyre at latitudes between 38°S and 25°S, reaching its easternmost position around 172°W. Similar findings were also reported by Holbrook and Maharaj (2008). It is interesting to note that the spatial pattern of the SPWSTMW thickness is similar to the depth of its lower limit, with its maxima exceeding 130 m around 156°E, 33°S and 172°E, 30°S, and decreases dramatically to both southward and northward, forming a front at latitudes between about 36°S and 40°S. Tsubouchi et al (2007) also found that there are two separate thickness maxima located around 160° and 175°E in the 25-30°S latitudinal band, which are located further equatorward than those from the present study. As shown in Figure 3d, the SPWSTMW thickness reaches its seasonal maximum in October, and then drops toward its seasonal minimum in May. This seasonal pattern is consistent with the result of Holbrook and Maharaj (2008) in terms of the SPWSTMW volume.

Seasonal variation of potential temperature averaged over the region where the SPWSTMW is identified and thermostad is thicker than 40 m is shown in Figure 4. From December to May, isotherms (14-20°C) of the SPWSTMW lie between 60 m and 330 m below the mixed layer. The most pronounced feature of this seasonal variation is related to the buoyancy loss in winter, which erodes the summer mixed layer, causing the 20 °C isotherm to outcrop. The outcropping of the 20 °C isotherm marks the opening of a ventilation window, where some portion of the SPWSTMW is exposed to the atmosphere. However, this outcropping process is not shown by Fernandez et al's (2017) results (e.g., their Figure 4b). A possible cause for this discrepancy lies in the fact that their analysis was based on a single transect along 176.5°E, not on the data over the entire region of the SPWSTMW. By the end of November, the surface layer begins to restratify, which isolates the SPWSTMW from the surface layer.

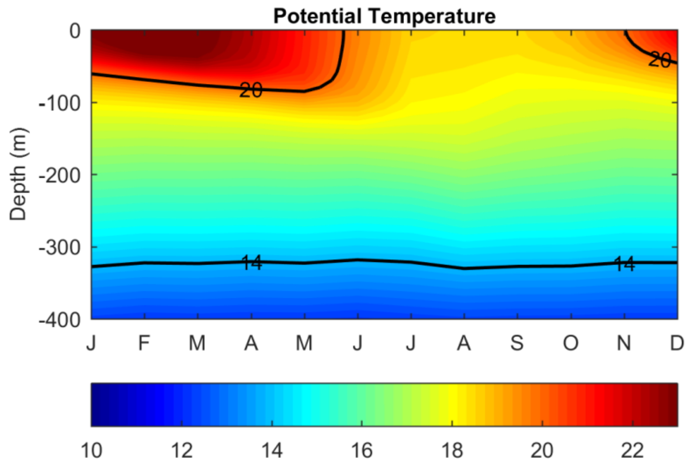

Figure 4. Seasonal cycle of potential temperature averaged over the region where the SPWSTMW is present. The isotherms (14 °C and 20 °C) used to define the potential temperature range of the SPWSTMW are shown.

Previous studies have shown that stratification is an important factor influencing the formation of the mode water (Ladd & Thompson, 2000; Luo et al., 2009). Hence, it is worthwhile to examine the impact of stratification on the SPWSTMW. Figure 5 shows the monthly mean vertical temperature gradient along the 173°E section, crossing the maximum thickness of the SPWSTMW. Surface stratification starts to vanish in June as a result of surface cooling, and this is consistent with a decreasing vertical temperature gradient near the surface (Figure 5). The newly formed

SPWSTMW is clearly evident south of 35°S in July. In the subsequent months, the newly formed SPWSTMW continues to subduct between the 14 °C and 20 °C isotherms and extends northward to about 24°S in the depth range between 100 m and 260 m until November, indicating an equatorward spreading of the SPWSTMW. Using the DASPOT dataset, Holbrook and Maharaj (2008) have also shown that the SPWSTMW can extends equatorward to near 24°S along a similar meridional section around 177°E (e.g., their Figure 3a). Starting from November, strong sea surface heating and weak surface wind restratify the surface mixed layer. With the development of surface stratification, the SPWSTMW is gradually detached from the surface mixed layer. During the period from December to the following March, when surface stratification is most developed, the vertical extent of the SPWSTMW steadily shrinks. During the dissipation period from April to June, the SPWSTMW continues to shrink and almost disappears in June. In general, this seasonal evolution of the SPWSTMW is in line with the result of Holbrook and Maharaj (2008) based on DASPOT dataset.

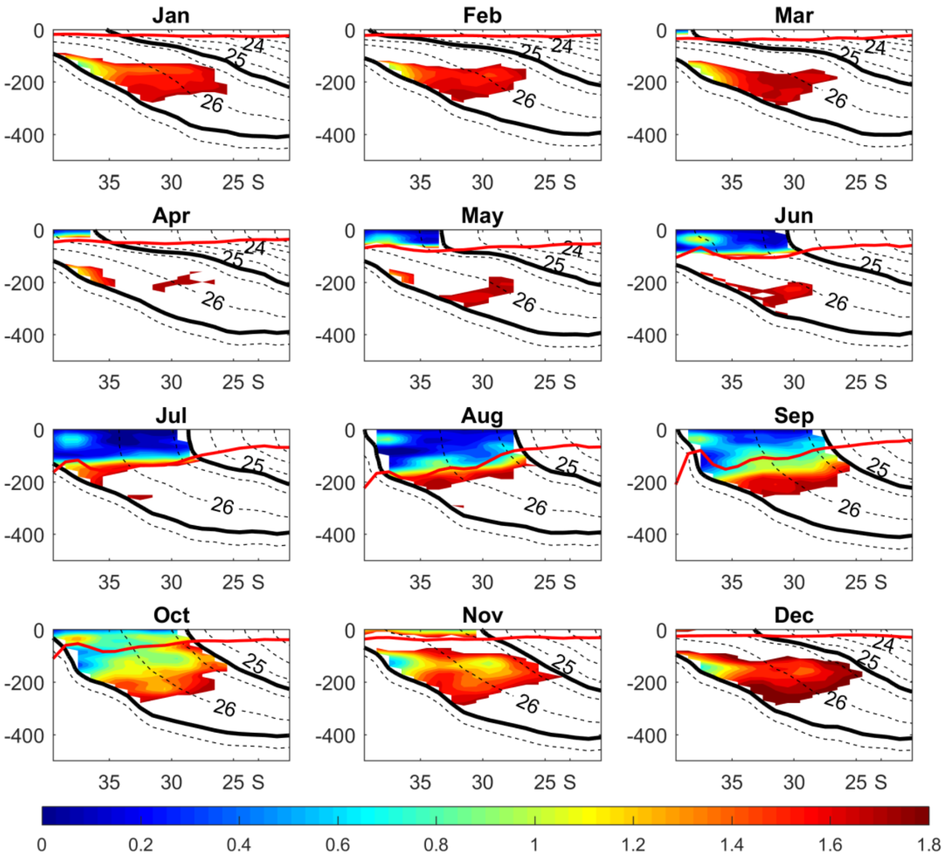

Figure 5. Monthly climatology (shading) of vertical temperature gradient (≤1.8 ℃/100m) along the 173°E section during 2004-2018 from RG09 data product. The black thick solid lines indicate the 14 ℃ and 20 ℃ isotherms, the light dashed lines indicate potential density with a contour interval of 0.5 kg/m^3, and the red thick line indicates the MLD.

Considering that volume of a water mass is an important physical parameter describing the intensity of ocean ventilation, our discussion below focuses on the variability of the SPWSTMW volume. The annual cycle of the SPWSTMW volume can be divided into three distinct periods: the formation period, the isolation period, and the dissipation period. The formation of new SPWSTMW occurs primarily in late austral winter and early spring (from June to October). During the isolation period (from November to the following February), the SPWSTMW is gradually detached from the surface mixed layer (Figure 5). The dissipation of SPWSTMW usually occurs from March to May, during this period, the SPWSTMW remains submerged beneath the surface and continues to dissipate until a new formation season (Figure 6a). As a key factor influencing the formation of the SPWSTMW, we first show the MLD averaged over the SPWSTMW formation regions (Figure 6a). Here, we define the SPWSTMW formation region as the surface region where surface water lie between the 14 and 20 °C isotherms and where vertical potential temperature gradient is less than 1.8 °C/100m. The MLD starts to deepen in April, and reaches its seasonal maximum in August. In accordance with the deepening MLD, the SPWSTMW is formed in austral winter (June-September). During this formation season, the SPWSTMW volume gradually increases, reaching its seasonal maximum of 6.15 (±0.72) $\times10^5$ km^3 in October. The MLD starts to shoal in November, and the shoaling of the MLD continues throughout the austral summer (January-March). As a consequence, the SPWSTMW volume decreases from December to June, approaching its seasonal minimum of 1.82 (±0.51) $\times10^5$ km^3 in June, which is consistent with the earlier work by Holbrook and Maharaj (2008). Approximately, 71% of the SPWSTMW formed in October dissipates in the following 8 months, suggesting that a large portion of the SPWSTMW barely persists until the next winter, as previously suggested by Holbrook and Maharaj (2008) and Fernandez et al. (2017). The relatively short lifetime of the SPWSTMW explain why the SPWSTMW volume reaches its seasonal minimum in the dissipation period. The eroded SPWSTMW cannot be conveyed into the South Pacific subtropical gyre too far due to its short lifetime.

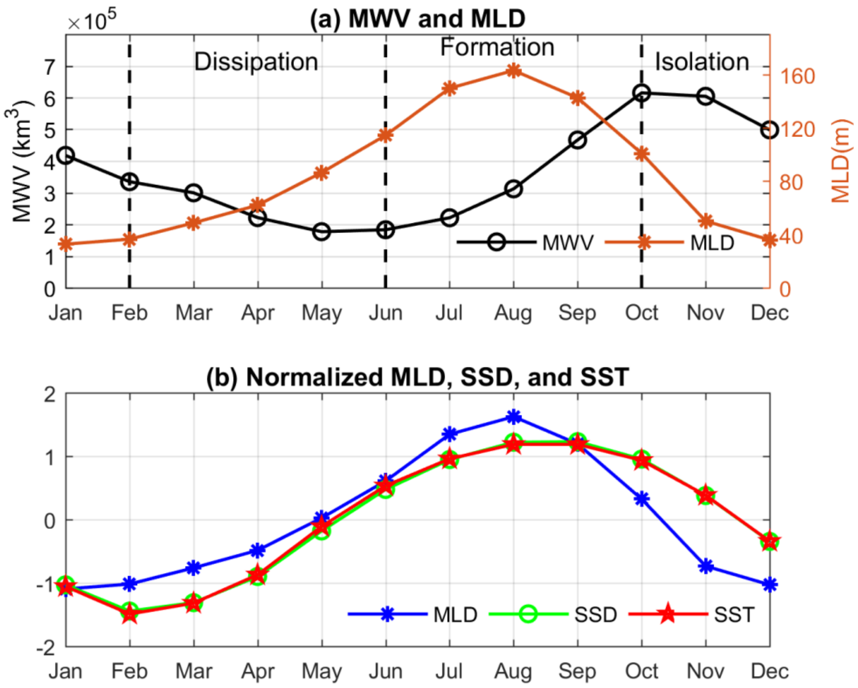

Figure 6. (a) Seasonal variation of the total SPWSTMW volume (km^3) and MLD (m) and, (b) the normalized MLD, SSD, and SST (sign-reversed) in the SPWSTMW formation region.

As discussed above, seasonal variation of the MLD plays an important role in modulating the SPWSTMW volume (Qu et al., 2002; Luo et al., 2011). Some earlier studies have shown that variability in the MLD is largely due to variability in sea surface density (SSD), which in turn is primarily caused by changes in surface heat flux and wind forcing (Luo et al., 2009, 2011; Qu et al., 2016). Here, we show that seasonal variations of the normalized SSD and MLD averaged over the SPWSTMW formation region are nearly identical (Figure 6b), giving additional support for the earlier speculation. In addition, the seasonal variation of SST (sign-reversed) is in exactly the same phase as that of SSD, implying that the seasonal variation of SSD in the SPWSTMW formation region is, to a great extent, thermal-driven. In other words, changes in SST dominate the seasonal variation of SSD and consequently the seasonal variation of the MLD. Furthermore, changes in SST in turn are primarily forced by changes in surface heat flux. Thus, we conclude that on seasonal timescale, local surface heat flux is the dominant process governing the MLD variability in the SPWSTMW formation region.

4 Interannual variability and its relationship with ENSO

Besides the seasonal cycle discussed above, a remarkable interannual variability in the SPWSTMW volume is also identified (Figure 7). To extract the dominant signal of this interannual variability, time series of the SPWSTMW volume is filtered by a 13-month moving average. The long-term trend of the SPWSTMW volume is also removed before the analysis. As shown in Figure 7, the SPWSTMW volume was higher during the periods of 2004/2005, 2006/2007, 2009/2010, and 2015/2016 and lower during the periods of 2007/2008, 2010/2011, and 2011/2012. This interannual variability shows the same phase as the SOI, with their correlation coefficient reaching -0.56 for the period of observation (2004-2019), satisfying the 95% confidence level. The SPWSTMW volume is observed to increase during El Niño periods but decrease during La Niña periods. The results show that the largest anomalies of the SPWSTMW volume occurred in 2010-2011 and 2015-2016, coinciding with the 2010/2011 La Niña event and 2015/2016 El Niño event, respectively, which is consistent with the earlier work by Fernandez et al. (2017) in terms of the SPWSTMW inventory north of New Zealand. These results corroborate earlier studies and suggest that both the oceanic and atmospheric processes associated with ENSO play an important role in governing the SPWSTMW variability on interannual timescales (Holbrook & Maharaj, 2008; Wang et al., 2015; Fernandez et al., 2017). The possible mechanisms responsible for the SPWSTMW variability, particularly its relationship with ENSO are examined below.

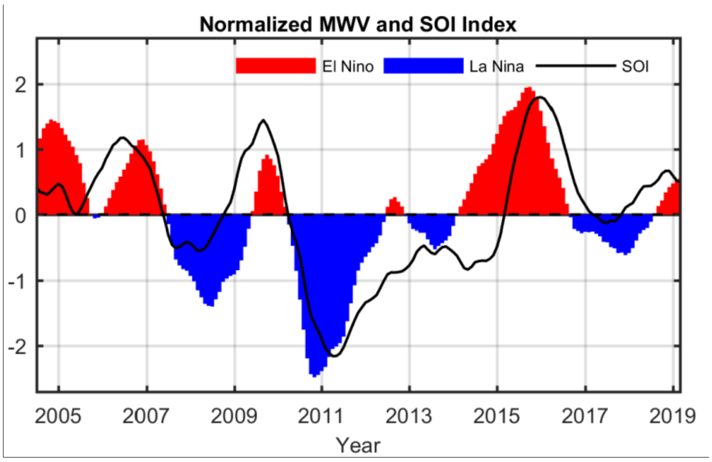

Figure 7. Comparison of the monthly mean SPWSTMW volume and SOI (sign-reversed). Both time series are normalized by the respective standard deviations. A 13-month moving average has been applied to remove the seasonal cycle, and the long-term trends are also removed.

As discussed above, MLD has a notable impact on the variability of the SPWSTMW volume on seasonal timescale. With this in mind, we first examine the relationship between the SPWSTMW volume and the MLD in the SPWSTMW formation region on interannual timescales. Since the maximum MLD occurs in late winter (Figure 6), we compare the MLD of August with the SPWSTMW volume averaged between September and October. The result shows a significant interannual variability in both time series, with their correlation coefficient reaching 0.6, satisfying the 95% confidence level (Figure 8). Previous studies suggested that formation of the STMW consists of two components: vertical pumping at the base of the winter mixed layer and lateral induction induced by the late winter MLD variability (Huang & Qiu, 1998). In general, the latter is thought to play a more important role than the former in governing the STMW variability (Qu et al., 2008). The close correlation between the SPWSTMW volume and MLD indicates that interannual variability of the SPWSTMW volume is primarily caused by changes in winter MLD through lateral induction (Figure 8a). In addition, time series of the normalized winter (August) SSD averaged over the SPWSTMW formation region is also presented in Figure 8b. From 2004 to 2019, the normalized winter SSD shows exactly the same phase as the normalized MLD, indicating that the SSD is a key factor controlling the MLD variability in the SPWSTMW formation region. In most cases, an increase in SSD leads to a deepening of MLD, and a decrease in SSD leads to a shoaling of MLD. Moreover, normalized winter SST (sign-reversed) exhibits exactly the same interannual variability as normalized winter SSD, indicating that, on interannual timescales, changes in SSD are primarily thermal-driven (Figure 8b). In contrast, changes in SSS contribute little to changes in SSD. In other words, it is the SST variability that dominates the MLD variability in the SPWSTMW formation region, which in turn is primarily caused by surface heat flux. Anomalous surface heat fluxes during the cool seasons (April to August) may first alter the SST, then the SSD, and eventually the MLD (Figure 8b).

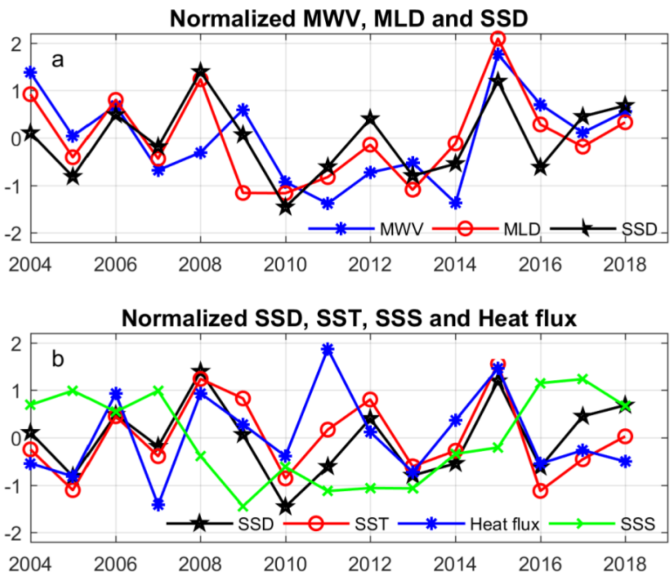

Figure 8. (a) Normalized year to year variability of the SPWSTMW volume in September-October and the MLD, SSD in August, and (b) the SSD, SST (sign-reversed), and SSS in August, and surface heat flux (sign-reversed) in April-August averaged in the SPWSTMW formation region. A positive surface heat flux value indicates heat gain by the ocean, and vice versa.

Previous studies showed that variability in SST around New Zealand is closely related to ENSO (Sprintall et al., 1995; Mullan, 1998; Sutton & Roemmich, 2001), which tends to be cooler and leads to more SPWSTMW formed in the southwestern subtropical Pacific during El Niño years. To further investigate this relationship, we perform empirical orthogonal function (EOF) analyses of SST, net surface heat flux, and latent heat flux anomalies in the South Pacific. Only the first three EOF modes are considered here. The first EOF of SST explains about 48.5% of the total variance while the second and third EOF explains 22.0% and 10.7% respectively. As shown in Figure 9a, the first EOF mode of SST exhibits a notable interannual variability during the period 2004-2019, with negative values over the whole SPWSTMW formation region. Its time series corresponds well with the SOI, with their correlation coefficient reaching -0.68, satisfying the 95% confidence level. This suggests that SST in the SPWSTMW formation region gets cooler during El Niño years and warmer during La Niña years. The first EOF mode of net surface heat flux is also closely related to the SOI, with their correlation coefficient reaching -0.70, which is significant at the 95% confidence level.

Further inspection of the NCEP re-analysis products indicate that, among the four components of surface heat flux (i.e., latent heat flux, sensible heat flux, solar radiation, and long wave radiation), contribution from latent heat flux is dominant. In contrast, the spatial pattern of the first EOF mode of latent heat flux is similar to that of net surface heat flux, indicating that latent heat flux anomalies are primarily responsible for anomalous SST on interannual timescales.

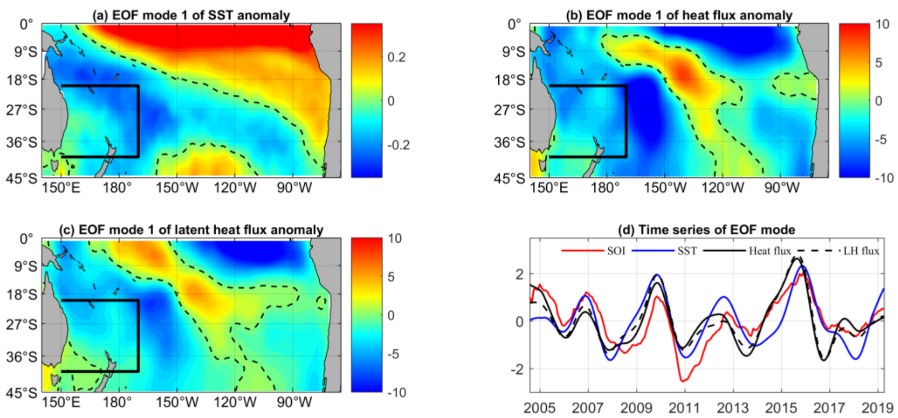

Figure 9. Spatial distribution and time series of the first EOF mode of (a) SST (°C), (b) net surface heat flux (W/m^2), and (c) latent heat flux (W/m^2) anomalies. (d) The first EOF time series of the SST (blue solid line), net surface heat flux (black solid line), latent heat flux (black dashed line), and the SOI (red solid line, sign-reversed). The black box represents the study region; the black dashed line denotes the zero line of each variable. All data are filtered by a 13 months moving average.

The question that arises immediately is how ENSO remotely influences SST in the southwestern subtropical Pacific. Luo et al. (2011) suggested that SST in the southeastern subtropical Pacific can be modulated by surface winds. Enhanced surface winds can lead to more heat loss from the ocean to the atmosphere through the wind-evaporation-SST (WES) feedback mechanism (Xie et al., 2010). Based on these earlier studies, we hypothesize that, ENSO-related wind anomalies maybe a major driver of SST anomalies in the southwestern subtropical Pacific on interannual timescales. Latent heat flux is of particular importance to the WES feedback mechanism. To test this hypothesis, we perform an empirical orthogonal function (EOF) analysis of wind speed. The first EOF mode of wind speed exhibits interannual variations during the period 2004-2019 (Figure 10a), with positive anomalies covering most parts of the SPWSTMW formation region. Moreover, the time series of the first EOF mode of wind speed shows a good correlation with the SOI, with a correlation coefficient of -0.75 (exceeding 95% confidence level) (Figure 10b). This result suggests that wind in the SPWSTMW formation region gets stronger than normal during the El Niño period (negative phases of SOI) and vice versa. Moreover, the first EOF mode of wind speed shows a similar spatial pattern to that of the reverse-sign SST anomaly (Figure 9a). This indicates that, in the SPWSTMW formation region, variability of SST is mainly caused by anomalous local wind through the WES feedback mechanism. Beside the local wind, ocean dynamic processes, such as Ekman transport due to anomalous wind, may also play a role in moderating SST variability (Wang et al., 2015).

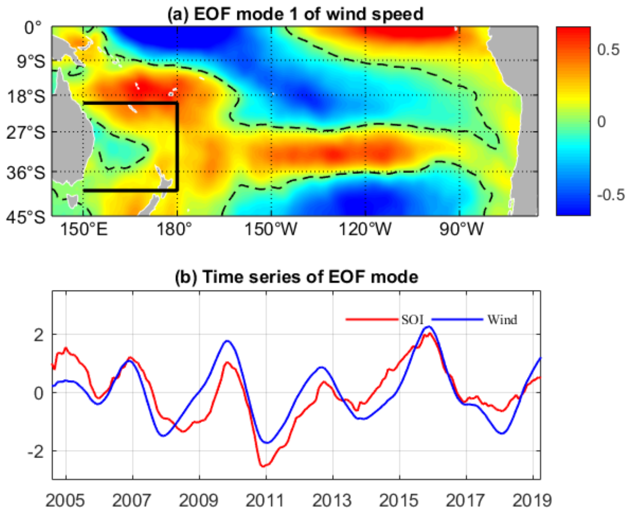

Figure 10. Same as for Figure 9 but for wind speed anomalies (m s^{-1})

To further illustrate the impact of ENSO on SPWSTMW variability, we conducted a composite analysis of wind anomalies for El Niño years. Considering that the MLD in the South Pacific reaches its maximum in August and the oceanic response to surface wind anomalies lags by 2-3 months, we use wind speeds averaged between May and June to represent the late austral autumn and early winter winds. Based on the NOAA's definition, there are four El Niño events (2004/2005, 2006/2007, 2009/2010, and 2015/2016) during the period 2004-2019. As shown in Figure 11a, the climatological surface winds in late austral autumn and early winter (May-June) east of Australia show an anticyclonic rotation of the annual mean winds from southwestward to southeastward. When an El Niño develops in May-June, positive SST anomalies in the central-eastern equatorial Pacific induce a Gill-Matsuno-type wind response (Gill, 1980), with cyclonic wind anomalies north of New Zealand. These cyclonic wind anomalies cause anticyclonic wind anomalies east of Australia (Figure 11b). These anomalous winds enhance the local winds in the southwestern subtropical Pacific, resulting directly in an increase in latent heat flux, more heat loss from the ocean to the atmosphere, and finally a decrease in SST (Figure 11c). The SST cooling further induces deeper MLD in the SPWSTMW formation region (Figure 11d). Furthermore, during an El Niño event, upper ocean stratification gets weaker due to stronger than normal wind stirring and heat loss to the atmosphere. This also provides a favorable condition for the development of a deeper mixed layer and hence a stronger SPWSTMW formation.

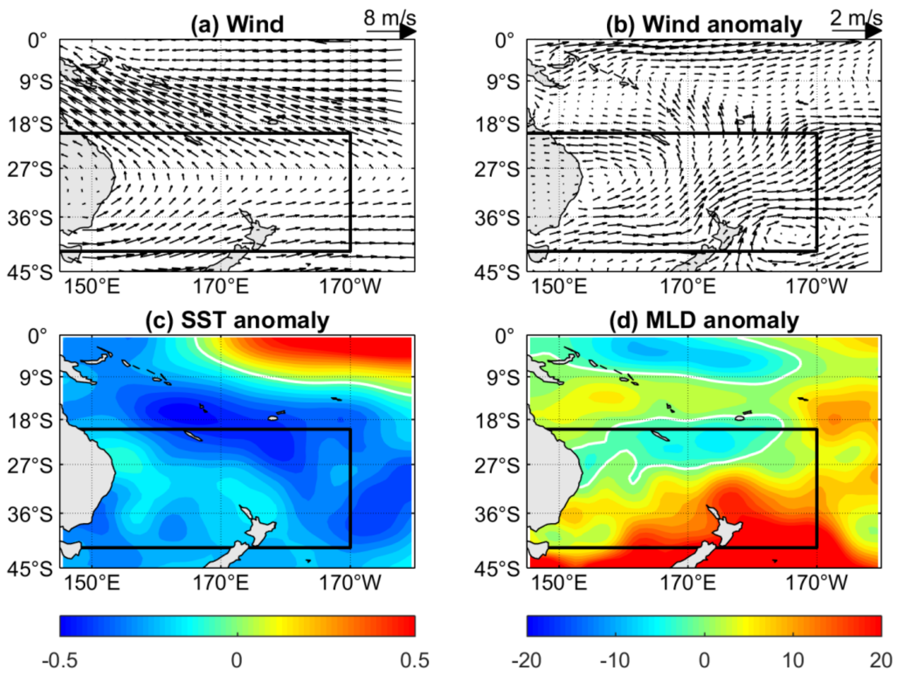

Figure 11. (a) Climatological mean (May-June) surface wind speed (m/s), (b) composite of surface wind speed (m/s) anomalies during El Niño years in late austral autumn and early winter (May-June), (c) SST anomalies (August), and (d) MLD anomalies (August). The white solid lines denote the zero line of each variable.

As discussed above, during El Niño years, surface winds in the SPWSTMW formation region are stronger than during normal years. This enhances evaporation and leads to more heat loss to the atmosphere, causing a decrease in SST through the

WES feedback mechanism (Xie et al., 2010). The reduced SST further decreases stratification and deepens the MLD. The deepening of the MLD in the SPWSTMW formation region then enhances the horizontal MLD gradients and consequently the lateral induction and subduction of the SPWSTMW, directly contributing to the increase of the SPWSTMW volume. The situation is reversed during La Niña years.

Recently, a new type of El Niño has emerged from the conventional eastern Pacific (EP) El Niño, referred to as El Niño-Modoki (Ashok et al., 2007; Freund et al. 2019), or central Pacific El Niño (Yu & Kim, 2010). Because of different SST anomaly patterns and intensities, remarkable differences exist in atmospheric circulation anomalies between the two types of El Niño. Then, an interesting question arises whether the SPWSTMW responds to CP El Niño and EP El Niño differently? During the period 2004-2019, two strong El Niño events occurred. One was in 2009/2010, and the other in 2015/2016, representing the CP and EP El Niño, respectively. As shown in Figure 7, although both CP and EP El Niño events can lead to an increase in SPWSTMW volume, there are still some differences in timing phase between the two types of El Nino events. For example, during the 2009/2010 event, the anomalies of the SPWSTMW volume peaked earlier than the mature phase of El Niño by 1-2 months. However, for the 2015/2016 event, the anomalies of the SPWSTMW volume peaked after the mature phase of El Niño by 2-3 months. This question deserves further investigation in future studies.

5 Summary and Discussion

This study utilizes a gridded Argo data product from January 2004 to September 2019 to explore the variability of the SPWSTMW volume and its relationship with ENSO. Our results show that the mean thickness of the SPWSTMW is about 62 (± 10) m, with its upper and lower boundary lying at about 60 m and 330 m, respectively. Two local maxima (both exceeding 130 m) are identified. One lies around 156°E and 33°S, and the other near 172°E and 30°S.

The SPWSTMW volume exhibits significant variations on seasonal and interannual timescales. On the seasonal timescale, the SPWSTMW volume shows three distinct periods: the formation period (June-October), the isolation period (November-February), and the dissipation period (March-May). The SPWSTMW volume reaches its seasonal maximum of 6.15 (±0.72) $\times 10^5$ km^3 in October and minimum of 1.82 (±0.51) $\times 10^5$ km^3 in June. This agrees well with the findings of Holbrook and Maharaj (2008), who found that the SPWSTMW volume (west of 180°) varies from a maximum of 6.6 (±0.5) $\times 10^5$ km^3 in October to a minimum of 1.9 (±0.4) $\times 10^5$ km^3 in May based a different observation data (DASPOT). Approximately, 71% of the SPWSTMW formed in austral winter dissipates in the following seasons, suggesting that the SPWSTMW hardly persists toward the next winter. The short lifetime of SPWSTMW indicates that this water mass is mostly confined to southwestern subtropical Pacific and not advected to locations very remote from the formation region.

A remarkable interannual variability is identified in the SPWSTMW volume. This variability is closely related to changes in the wintertime MLD. Surface heat flux plays a dominate role in controlling the SPWSTMW volume variability through its modulation of the MLD. More importantly, the interannual variability of the SPWSTMW volume exhibits a significant ENSO signal, with positive anomalies during El Niño periods and negative anomalies during La Niña periods. Such a link between the SPWSTMW volume and ENSO has also been observed by previous studies, such as Holbrook and Maharaj (2008) and Fernandez et al. (2017), based on different observations during different periods of time.

Further analyses of surface wind, SST, surface heat flux, and latent heat flux anomalies indicate that during El Niño periods, positive SST anomalies in the equatorial central-eastern Pacific induce a Gill-Matsuno-type wind feedback (Gill, 1980), with anomalous winds enhancing the local winds, resulting in a decrease in SST through the WES feedback in the SPWSTMW formation region (Xie et al., 2010). It should be noted that the WES feedback is a two-way interaction between wind and SST. For example, Marshall et al. (2015) argued that the local SST anomalies induced rainfall and sea level pressure adjustment in the western Australian coast can further affect the regional wind anomalies through a positive WES feedback mechanism. Similarly, the negative SST anomaly to the north of the SPWSTMW formation region can induces a Gill-Matsuno-type atmospheric response with an anti-cyclonic circulation at the southwest side of the negative SST anomalies center (Figure 11), thereby acting to further enhance the anti-cyclonic wind anomalies and surface cooling (Gill, 1980). Enhanced surface cooling and wind stirring deepen the MLD and eventually leave an imprint of ENSO on the SPWSTMW through lateral induction.

Recently, Fernandez et al. (2017) found that the SPWSTMW inventory north of New Zealand prior to 2000 was weakly correlated with ENSO, but their correlation became significantly higher after 2000. Why this change happens has not been explained yet. Some recent studies have indicated that, a decadal change in ENSO cycle recently occurred around 2000, toward weaker-amplitude, higher-frequency, and increased occurrence of CP El Niño events (Ashok et al, 2007; Yeh et al., 2009; Lee & McPhaden, 2011; McPhaden, 2012; Lübbecke & Mcphaden, 2014; Freund et al. 2019). Interestingly, this change in ENSO cycle is consistent with that in relationship between the SPWSTMW and ENSO. Then, are there any connections between the increased correlation noted above after 2000 and the change in ENSO cycles (especially the CP El Niño events)? Holbrook and Maharaj (2008) reported that the relationship between the SPWSTMW and ENSO can be modulated by decadal climate variability. Taschetto et al. (2009) also reported that the Australian monsoon is more sensitive to positive SST anomalies in the central Pacific than those in the eastern Pacific. Based on these results from previous studies, we propose a possible explanation for this change in relationship between the SPWSTMW and ENSO around 2000. The increased relationship between the SPWSTMW and ENSO after 2000 may be caused by a higher occurrence of anomalous warming events associated with El Niño in the equatorial central Pacific. During the developing phase of an El

Niño event, positive SST anomalies in the central-eastern Pacific can induce a Gill-Matsuno type wind feedback, strengthening the surface winds and enhancing the SPWSTMW formation in the southwestern subtropical Pacific. Apparently, this question can't be addressed using the Argo data along, and it requires further investigation in future studies by using long-term reanalysis data and/or model outputs.

Finally, we note that the variability of the SPWSTMW volume and SOI are not completely in phase, suggesting that the ENSO is not the sole process governing the variability of the SPWSTMW volume. Other processes, such as instabilities in the East Australian Current and mesocale eddies, may also play a role (Qiu et al., 2007; Oka et al., 2009; Xu et al., 2014; Wang et al., 2015). We will investigate these issues in future studies.

Acknowledgments

J. Qi was supported by the Strategic Priority Research Program of Chinese Academy of Sciences (XDB42000000), the National Natural Science Foundation of China (41506020). T. Qu was supported by the National Science Foundation (1829809). B. Yin was supported by the NSFC-Shandong Joint Fund (U1806227), the National Key Research and Development Program of China (2017YFA06041021), the National Basic Science and Technology Program of China (2013FY111300). The authors are grateful to R.H. Xie for useful discussion on the topic and to three anonymous reviewers for their helpful comments which improved the manuscript. The Argo data were collected and made freely available by the International Argo Program and the national programs that contribute to it. (http://www.argo.ucsd.edu, http://argo.jcommops.org). The Argo Program is part of the Global Ocean Observing System. NCEP Reanalysis Derived data was provided by the NOAA/OAR/ESRL PSD, Boulder, Colorado, USA, from their web site at https://www.esrl.noaa.gov/psd/. The ERA-Interim reanalysis data were obtained from the European Centre for Medium-Range Weather Forecasts (https://www.ecmwf.int/en/forecasts/datasets/reanalysis-datasets/era-interim). The monthly Southern Oscillation Index (SOI) was obtained from the Australian Government Bureau of Meteorology (http://www.bom.gov.au/climate/current/soi2.shtml).

References

Alexander, M. A., Bladé, I., Newman, M., Lanzante, J. R., Lau, N. C., & Scott, J. D. (2002). The atmospheric bridge: The influence of ENSO teleconnections on air-sea interaction over the global oceans. *Journal of Climate, 15*, 2205-2231. https://doi.org/10.1029/2001GL014347.

Ashok, K., Behera, S. K., Rao, S. A., Weng, H., & Yamagata, T. (2007). El Niño Modoki and its possible teleconnection. *Journal of Geophysical Research: Oceans, 112(C11)*. https://doi.org/10.1029/2006JC003798

Dee, D. P., Uppala, S. M., Simmons, A. J., Berrisford, P., Poli, P., Kobayashi, S., et al. (2011). The ERA-Interim reanalysis: Configuration and performance of the data assimilation system. *Quarterly Journal of the Royal Meteorological Society, 137*(656), 553-597. https://doi.org/10.1002/qj.828

Drushka, K., Sprintall, J., & Gille, S. T. (2014). Subseasonal variations in salinity and barrier-layer thickness in the eastern equatorial Indian Ocean. J*ournal of Geophysical Research: Oceans, 119*(2), 805-823. https://doi.org/10.1002/2013JC009422

Fernandez, D., Sutton, P., & Bowen, M. (2017). Variability of the subtropical mode water in the Southwest Pacific. *Journal of Geophysical Research, 122*(9), 7163-7180. https://doi.org/10.1002/2017JC013011

Freund, M., Henley, B. J., Karoly, D. J., Mcgregor, H., Abram, N. J., & Dommenget, D. (2019). Higher frequency of Central Pacific El Nino events in recent decades relative to past centuries. *Nature Geoscience, 12*(6), 450-455. https://doi.org/10.1038/s41561-019-0353-3

Gill, A. E. (1980). Some simple solutions for heat-induced tropical circulation. *Quarterly Journal of the Royal Meteorological Society, 106*(449), 447-462. https://doi.org/10.1002/qj.49710644905

Hanawa, K., &Talley, L. (2001). Mode Waters, in Ocean Circulation and Climate, Int. Geophys. Ser., vol. 77, edited by S. Siedler, J. Church, and J. Gould, pp. 373-386, Academic, San Diego, Calif.

Holbrook, N. J., & Bindoff, N. L. (2000a). A Statistically Efficient Mapping Technique for Four-Dimensional Ocean Temperature Data. *Journal of Atmospheric* *and Oceanic Technology, 17*(6), 831-846. https://doi.org/10.1175/1520-0426(2000)017<0831:ASEMTF>2.0.CO;2

Holbrook, N. J., & Bindoff, N. L. (2000b). A digital upper ocean temperature atlas for the southwest Pacific: 1955-1988. *Australian Meteorological and Oceanographic Journal, 49*(1), 37-49.

Holbrook, N. J., & Maharaj, A. M. (2008). Southwest Pacific subtropical mode water: A climatology. *Progress in Oceanography, 77*(4), 298-315. https://doi.org/10.1016/j.pocean.2007.01.015

Huang, R. X., & Qiu, B. (1998). The structure of the wind-driven circulation in the subtropical South Pacific Ocean. *Journal of Physical Oceanography, 28*(6), 1173-1186.
https://doi.org/10.1175/1520-0485(1998)028<1173:TSOTWD>2.0.CO;2

Kalnay, E., Kanamitsu, M., & Kistler, R. (1996). The NCEP/NCAR 40-Year Reanalysis Project, Bull. Amer. *Meteor. Soc., 77*, 437-472 (Vol. 2).

Ladd, C., & Thompson, L. (2000). Formation mechanisms for North Pacific central and eastern subtropical mode waters. *Journal of Physical Oceanography, 30*(5), 868-887. https://doi.org/10.1175/1520-0485(2000)030<0868:FMFNPC>2.0.CO;2

Lee, T., & McPhaden, M. J. (2010). Increasing intensity of El Niño in the central-equatorial Pacific. *Geophysical Research Letters, 37*(14).https://doi.org/10.1029/2010GL

Li, Z. (2012). Interannual and decadal variability of the subtropical mode water formation in the South Pacific Ocean. *Ocean Modelling, 47*, 96-112. https://doi.org/10.1016/j.ocemod.2012.02.001

Lübbecke, J. F., & Mcphaden, M. J. (2014). Assessing the twenty-first-century shift in enso variability in terms of the bjerknes stability index. *Journal of Climate, 27*(7), 2577-2587. https://doi.org/10.1175/JCLI-D-13-00438.1

Luo, Y., Liu, Q., & Rothstein, L. M. (2009). Simulated response of North Pacific Mode Waters to global warming. *Geophysical Research Letters, 36*(23). https://doi.org/10.1029/2009GL040906

Luo, Y., Liu, Q., & Rothstein, L. M. (2011). Increase of South Pacific eastern subtropical mode water under global warming. *Geophysical Research Letters, 38*(1). https://doi.org/10.1029/2010GL045878

Marshall, A. G., Hendon, H. H., Feng, M., & Schiller, A. (2015). Initiation and amplification of the Ningaloo Niño. *Climate Dynamics. 45*, 2367-2385. https://doi.org/10.1007/s00382-015-2477-5

Mcphaden, M. J., Zebiak, S. E., & Glantz, M. H. (2006). ENSO as an Integrating Concept in Earth Science. *Science, 314*(5806), 1740-1745. https://doi.org/10.1126/science.1132588

McPhaden, M. J. (2012). A 21st century shift in the relationship between ENSO SST and warm water volume anomalies. *Geophysical Research Letters, 39*(9). https://doi.org/10.1029/2012GL051826

Mullan, A. B. (1998). Southern hemisphere sea-surface temperatures and their contemporary and lag association with New Zealand temperature and precipitation. *International Journal of Climatology: A Journal of the Royal Meteorological Society,* *18*(8), 817-840. https://doi.org/10.1002/(SICI)1097-0088(19980630)18:8<817::AID-JOC261>3.0.CO;2-E

Oka, E., Toyama, K., & Suga, T. (2009). Subduction of North Pacific central mode water associated with subsurface mesoscale eddy. *Geophysical Research Letters,* *36*(8). https://doi.org/10.1029/2009GL037540

Oka, E., & Qiu, B. (2012). Progress of North Pacific mode water research in the past decade. *Journal of oceanography,* *68*(1), 5-20. https://doi.org/10.1007/s10872-011-0032-5

Oka, E., Qiu, B., Takatani, Y., Enyo, K., Sasano, D., Kosugi, N., et al. (2015). Decadal variability of Subtropical Mode Water subduction and its impact on biogeochemistry. *Journal of Oceanography*， *71*(4), 389-400. https://doi.org/10.1007/s10872-015-0300-x

Qiu, B., Chen, S., & Hacker, P. (2007). Effect of mesoscale eddies on subtropical mode water variability from the Kuroshio Extension System Study (KESS). *Journal of Physical Oceanography,* *37*(4), 982-1000. https://doi.org/10.1175/JPO3097.1

Qu, T., Xie, S. P., Mitsudera, H., & Ishida, A. (2002). Subduction of the North Pacific mode waters in a global high-resolution GCM. *Journal of Physical Oceanography,* *32*(3), 746-763. https://doi.org/10.1175/1520-0485(2002)032<0746:SOTNPM>2.0.CO;2

Qu, T., Gao, S., Fukumori, I., Fine, R. A., Lindstrom, E. J. (2008). Subduction of south pacific waters. *Geophysical Research Letters, 35*(2). https://doi.org/10.1029/2007GL032605

Qu, T., Zhang, L., & Schneider, N. (2016). North Atlantic subtropical underwater and its year-to-year variability in annual subduction rate during the Argo period. *Journal of Physical Oceanography, 46*(6), 1901-1916. https://doi.org/10.1175/JPO-D-15-0246.1

Roemmich, D., & Cornuelle, B. (1992). The subtropical mode waters of the South Pacific Ocean. *Journal of physical oceanography, 22*(10): 1178-1187. https://doi.org/10.1175/1520-0485(1992)022<1178:TSMWOT>2.0.CO;2

Roemmich, D., Gilson, J., Willis, J., Sutton, P., & Ridgway, K. (2005). Closing the time-varying mass and heat budgets for large ocean areas: The Tasman Box. *Journal of Climate, 18*(13): 2330-2343. https://doi.org/10.1175/JCLI3409.1

Roemmich, D., & Gilson, J. (2009). The 2004-2008 mean and annual cycle of temperature, salinity, and steric height in the global ocean from the Argo Program. *Progress in Oceanography, 82*(2), 81-100. https://doi.org/10.1016/j.pocean.2009.03.004

Sato, K., & Suga, T. (2009). Structure and modification of the South Pacific Eastern Subtropical Mode Water. *Journal of Physical Oceanography, 39*(7), 1700-1714. https://doi.org/10.1175/2008JPO3940.1

Speer, K., & Forget, G. (2013). Global distribution and formation of mode waters. *In International Geophysics*. https://doi.org/10.1016/B978-0-12-391851-2.00009-X

Sutton, P. J., & Roemmich, D. (2001). Ocean temperature climate off north-east New Zealand. *New Zealand Journal of Marine and Freshwater Research, 35*(3), 553-565. https://doi.org/10.1080/00288330.2001.9517022.

Sprintall, J., Roemmich, D., Stanton, B., &Bailey, R. (1995). Regional climate variability and ocean heat transport in the southwest Pacific Ocean. *Journal of Geophysical Research: Oceans, 100*(C8), 15865-15871. https://doi.org/10.1029/95JC01664

Taschetto, A. S., & England, M. H. (2009). El Niño Modoki impacts on Australianrainfall. *Journal of Climate, 22*(11):3167-3174. https://doi.org/10.1175/2008JCLI2589.1

Taschetto, A. S., Ummenhofer, C. C., Gupta, A. Sen, & England, M. H. (2009). Effect of anomalous warming in the central Pacific on the Australian monsoon. *Geophysical Research Letters, 36*(12). https://doi.org/10.1029/2009GL038416

Taschetto, A. S., Gupta, A. Sen, Jourdain, N. C., Santoso, A., Ummenhofer, C. C., & England, M. H. (2014). Cold tongue and warm pool ENSO Events in CMIP5: Mean state and future projections. *Journal of Climate, 27*(8):2861-2885. https://doi.org/10.1175/JCLI-D-13-00437.1

Tsubouchi, T., Suga, T., & Hanawa, K. (2007). Three types of South Pacific subtropical mode waters: Their relation to the large-scale circulation of the South

Pacific subtropical gyre and their temporal variability. *Journal of Physical Oceanography, 37*(10), 2478-2490. https://doi.org/10.1175/JPO3132.1

Wang, X. H., Bhatt, V., &Sun, Y. J. (2015). Seasonal and inter-annual variability of western subtropical mode water in the South Pacific Ocean. *Ocean Dynamics, 65*(1), 143-154. https://doi.org/10.1007/s10236-014-0792-8

Wong, A. P. S., & Johnson, G. C. (2003). South Pacific Eastern subtropical mode water. *Journal of Physical Oceanography, 33*(7), 1493-1509. https://doi.org/10.1175/1520-0485(2003)033<1493:SPESMW>2.0.CO;2

Xie, S. P., Deser, C., Vecchi, G. A., Ma, J., Teng, H., & Wittenberg, A. T. (2010). Global warming pattern formation: Sea surface temperature and rainfall. *Journal of Climate, 23*(4), 966-986. https://doi.org/10.1175/2009JCLI3329.1

Xie, S. P., Xu, L., Liu, Q., & Kobashi, F. (2011). Dynamical role of mode water ventilation in decadal variability in the central subtropical gyre of the North Pacific. *Journal of Climate, 24*(4), 1212-1225. https://doi.org/10.1175/2010JCLI3896.1

Xu, L., Xie, S.-P., McClean, J. L., Liu, Q., & Sasaki, H. (2014). Mesoscale eddy effects on the subduction of North Pacific mode waters. *Journal of Geophysical Research: Oceans, 119*(8), 4867-4886. https://doi.org/10.1002/2014jc009861

Yeh, S. W., Kug, J. S., Dewitte, B., Kwon, M. H., Kirtman, B. P., & Jin, F. F. (2009). El Niño in a changing climate. *Nature, 461*(7263), 511-514.

Yu, J. Y., Kim, S. T., 2010. Three evolution patterns of central-Pacific El Niño. *Geophysical Research Letters, 37*(8). https://doi.org/10.1029/2010GL042810

Yu, J.Y., Wang, X., Yang, S., Paek, H. &Chen, M. (2017). The changing El Niño–Southern Oscillation and associated climate extremes (pp. 1-38). John Wiley & Sons, Inc., Hoboken, NJ, USA.

Yu, K., Qu, T., Dong, C., & Yan, Y. (2015). Effect of subtropical mode water on the decadal variability of the subsurface transport through the Luzon Strait in the western Pacific Ocean. *Journal of Geophysical Research: Oceans, 120*(10), 6829-6842. https://doi.org/10.1002/2015JC011016